LETTER | SEPTEMBER 29 2017

Velocity space degrees of freedom of plasma fluctuations

Sean Mattingly; Fred Skiff

Phys. Plasmas 24, 090703 (2017)
https://doi.org/10.1063/1.4996012
CHORUS

Velocity space degrees of freedom of plasma fluctuations

Sean Mattingly[1,a)] and Fred Skiff[2,b)]
[1]Department of Physics and Astronomy, University of Iowa, 212 Van Allen Hall, Iowa City, Iowa 52242, USA
[2]Department of Physics and Astronomy, University of Iowa, 504 Van Allen Hall, Iowa City, Iowa 52242, USA

(Received 13 July 2017; accepted 6 September 2017; published online 29 September 2017)

We present the first measurements of a plasma velocity-space cross-correlation matrix. A singular value decomposition is applied to this inherently Hermitian matrix, and the relation between the eigenmodes and the plasma kinetic fluctuation modes is explored. A generalized wave admittance is introduced for these eigenmodes. *Published by AIP Publishing.*
[http://dx.doi.org/10.1063/1.4996012]

Collective fluctuation modes of plasmas offer a general description of plasma dynamics in collisionless[1,2] and weakly collisional plasmas.[3] Kinetic modes have been studied both in low density plasmas[4–6] and in fusion plasmas, where in the latter, they play an important role in the energetics of electrostatic turbulence and transport.[7–9] Fluid and magnetohydrodynamic descriptions capture only a few modes in the full plasma collective mode spectrum. Understanding plasma fluctuations and transport requires the inclusion of kinetic modes. However, kinetic modes are difficult to isolate experimentally.

Detecting kinetic modes is best achieved by phase space resolving diagnostics. Here, we employ laser induced fluorescence (LIF)[10] to measure the plasma distribution fluctuation correlation function

$$C(\vec{x}_1, \vec{x}_2, \vec{v}_1, \vec{v}_2; \tau) = \langle \delta f(\vec{x}_1, \vec{v}_1, t) \delta f(\vec{x}_2, \vec{v}_2, t-\tau) \rangle_t, \quad (1)$$

where $\langle\rangle_t$ denotes a time average and $\delta f = (f - \langle f \rangle_t)$ is the phase space distribution function fluctuation.

Earlier LIF measurements of C found the autocorrelation given by the diagonal $v_1 = v_2$. Those measurements employed a single laser to measure fluorescence at two separate points along the laser beam[11] and to measure C as a function of single $v_1 = v_2$ with separation $x_1 - x_2$.[6] Bicoherence spectra were also derived from these measurements.[12] In this letter, we employ a local measurement technique with $x_1 = x_2$ and select two separate and adjustable velocities v_1 and v_2 so that a matrix of cross correlations can be obtained.

By doing this, we present in this letter the first measurements of a plasma velocity-space cross-correlation matrix. From this local measurement, multiple degrees of freedom can be isolated, including the kinetic modes. We validate our noise reduction techniques through the symmetry properties of the fluctuation correlation function. We demonstrate this technique on a weakly coupled plasma and compute the associated eigenvectors in velocity space. A frequency dependent generalized wave admittance can be derived for each eigenmode.

The locality of the measurement means that the technique may be applied to plasmas in which a single-point velocity-sensitive measurement is possible and multipoint measurements may be difficult. Examples include *in situ* measurements of space plasmas, fusion plasmas, trapped plasmas,[13] and laser cooled plasmas.[14]

While LIF is frequently used to measure slowly varying moments of the ion velocity distribution (n, $\vec{u}$, T, and higher), measuring fluctuations as required in this experiment is difficult due to photon statistics fluctuations that make a twofold contribution to noise. First, the LIF photon count rate is limited due to low metastable state densities and the need to avoid excessive optical pumping. Second, a large fraction of the light signal is not from single frequency LIF itself but rather from electron collision-induced fluorescence. Collision-induced fluorescence affects ions at all velocities and is related to the metastable state populating mechanisms. Thus, collision-induced fluorescence is linked to the signal magnitude. Therefore, a statistical subtraction is needed.

Correlation measurements use ensemble averaging which permits evaluation and elimination of photon statistics noise. Nevertheless, there is only the above mentioned handful of phase space incoherent fluctuation measurements. For this reason, the efficiency of subtraction of the background fluorescence is a secondary question that we address in this letter by exploiting symmetry properties of this correlation function.

The experiment is performed on an Argon II 13.56 MHz RF inductively coupled magnetized ($B \approx 0.067$ T) cylindrical plasma column of length 2.3 m and radius $r \approx 2.5$ cm.[6] A Langmuir probe measures the ion and electron densities $n \approx 9 \times 10^9\,\mathrm{cm}^{-3}$ and $T_e \approx 10$ eV. LIF reveals $T_i \approx 0.08$ eV, though there are significant deviations from a Maxwellian distribution. Ion neutral collisions have frequency $\nu \approx 500$ Hz. The ambient ion acoustic wave and drift wave amplitudes are above the thermal fluctuation level but are small due to convective stabilization. Additionally, a ring antenna driven with white noise excites broadband plasma modes in the system.

The experimental setup is shown in Fig. 1. Two separate lasers are combined using a dichroic mirror and sent into the plasma to induce fluorescence on two different metastable lines. These lines must be isolated—otherwise transitions between the excited states can affect the laser optical correlation. We have tested for this direct atomic collisional-radiative connection through extensive searches for laser modulation frequency mixing, which was not detected. The underlying form of these isolated LIF excitation schemes is

a)Electronic mail: frederick-skiff@uiowa.edu
b)Electronic mail: sean.w.mattingly@gmail.com

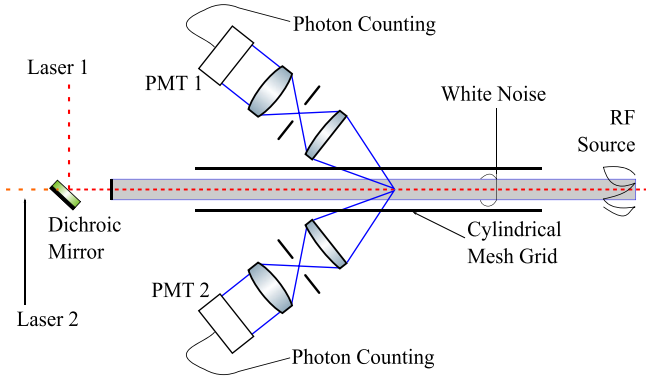

FIG. 1. Experimental data acquisition scheme and setup. Two lasers, one at 668 nm and one at 611 nm, are combined using a dichroic mirror and sent into the plasma. Corresponding to the two LIF schemes, PMT1 has a filter for 442 nm while PMT2 has a filter for 461 nm. An electrical white noise generator connected to a ring antenna excites the plasma modes with a broadband spectrum from 0 to 50 kHz. A cylindrical mesh grid gives additional definition to the radial mode structure.

the same: laser 1 excites the ArII metastable state $^4F_{7/2}$ with 668 nm to $^4D^\circ_{5/2}$ which decays to $^4P_{3/2}$, emitting light at 442 nm; laser 2 excites $^2G_{9/2}$ with 611 nm to $^2F^\circ_{7/2}$ which decays to $^2D_{5/2}$, emitting light at 461 nm. The dominant broadening mechanism of the laser absorption spectrum is Doppler broadening, and each laser absorption spectrum is broadened by the same plasma ion distribution function to within the noise level of 0.1%. Velocity selection is available with each tunable laser since the laser bandwidth is <1 MHz. Finally, to suppress the Zeeman pattern corresponding to the left circular polarization, these lasers are exclusively right circularized by passing them through a Glan-Taylor laser polarizer and a quarter wave plate. The low field of 0.067 T limits the width of each σ^+ polarized Zeeman group.

In this experiment, the collection optics are focused at the same point with a volume of 0.20 cm^3. Therefore, since the measurement scheme spatially combines the lasers and then obtains the correlation function at this physical volume, we obtain the correlation function of ions at two points separated in velocity phase space $C(v_1, v_2, \tau)$.

With this setup, first a full absorption spectrum is observed with each laser. We then choose a set of velocities across the distribution function: the peak of the distribution; 2/3 the peak of the distribution; 1/2 the peak; 1/3 the peak; and one point on the tail. The ion velocity distribution function's tail is due to how the plasma is produced,[15,16] In total, the same 8 velocity points are measured for each laser.

We then measure time series data $f(v, t)$ and $f(v', t)$ for the full array of selected velocities. After demodulation with respect to 100 kHz laser chopping, the mean is subtracted to provide the fluctuation $\delta f = f - \langle f \rangle_t$. Cross correlating and averaging $\delta f(v, t)$ and $\delta f(v', t-\tau)$ with respect to t give $C(v, v', \tau)$ for each of the selected velocities. This gives an $8 \times 8 \times (2N-1)$ matrix where the velocities form the first two axes and the time shift τ is the last axis.

During this process, photon statistics noise and background light are suppressed at several points: light filtering in the set up; background light subtraction through LIF signal demodulation (this step removes background light correlations as well); filtering via a Gaussian windowing function of the time cross correlation; and the suppression of photon statistics noise through averaging. In order to validate this noise reduction, we examine the correlation matrix.

Ideally, the matrix of correlation functions obeys the symmetry $C(v, v', \tau) = C(v', v, -\tau)$. However, this symmetry will not apply perfectly. There are small errors in wavelength selection, and the applied magnetic field induces slightly different Zeeman broadening for each laser absorption profile. This breaks the velocity space symmetry. However, keeping the magnetic field at 0.067 T ensures that the Zeeman subgroup is small compared to the measurement spacing. This is shown by the near symmetry of the actual raw data matrix.

Drift waves also help evaluate the degree of broken symmetry of the matrix. Consider the physical set up: the periscopes shown in Fig. 1 are oriented at 90° to each other and each has two cones of light collection volume with concurrent tips at the focus—where the lasers are located. The drift wave amplitude peaks in the gradient region of the plasma—higher up in the cone and away from the focus. With the physical setup in mind, we quantify how the matrix symmetry can be broken. The strongest drift wave mode corresponds to the first Fourier mode decomposition $e^{im\phi}$ where $m = 1$.[17] We check this by separating the matrix into symmetric and antisymmetric components $S, A = \frac{1}{2}(C(v_i, v_j; \tau) \pm C(v_j, v_i; -\tau))$ and taking the Fourier transform along the time axis to acquire $\tilde{S}, \tilde{A}$. These matrices, after this Fourier transform, are Hermitian and antihermitian by construction. Figure 2 shows a representative power spectrum from the matrix and its unwrapped phase. The unwrapped phase is $\pi/2$, and since the periscopes are positioned to have their light collection cones at angle $\pi/2$, this result is expected. The drift wave represents a worst case of broken data matrix Hermiticity, and the effect is mostly constrained in frequency space to the region around $f^* \approx 10$ kHz as shown in Fig. 2.

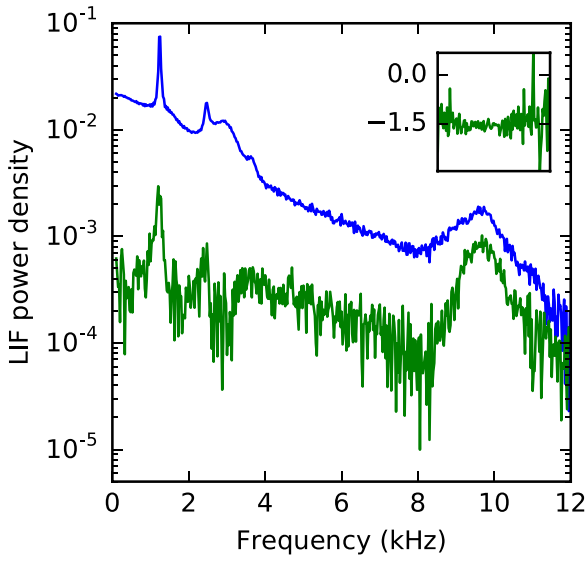

FIG. 2. Representative power spectrum of a single velocity pair's time cross correlation. The larger blue spectrum is the Hermitian component while the smaller green spectrum is the antihermitian component. The inset shows the phase of the antihermitian component at the drift frequency and has the same abscissa as the outer figure.

The spectra in Fig. 2 show that the Hermiticity of the matrix remains good to at least 10 dB for nearly all frequencies lower than the drift wave. This validates our noise reduction processes for this frequency range. This also provides a second validation that the Zeeman broadening is not too large.

Obtaining the plasma degrees of freedom and the plasma modes is now possible. We apply a singular value decomposition (SVD),[18,19] to the 2*D* Hermitian velocity matrix $\tilde{S}$ for every point in the frequency spectrum. The SVD gives the effective rank, or detected degrees of freedom, of the matrix at a given frequency by the number of singular values above the noise level. The magnitude of each singular value determines the relative importance of its corresponding principal axis. Assuming the continuity of the principal axes in frequency, we connect the singular values across the spectrum. The results are shown in Fig. 3. The strongest singular value mode spectrum is qualitatively similar to the undecomposed spectrum of Fig. 2.

However, SVD does not come without drawbacks. It assumes linearity and imposes the ansatz that the basis vectors are orthogonal. The basis of the ion velocity space distribution function may not always fulfill these assumptions. This is inextricably tied to SVD's strength: it does not make any other assumptions about the form of these basis vectors—which is why we use it here.

For comparison with the experiment, consider electrostatic ion waves where the plasma is quasineutral and the electron density follows a Boltzmann distribution. Rewriting the linearized Vlasov equation with a Poisson bracket, expanding in the gyrophase coordinate φ around the ion guiding centers, using a Bhatnager-Gross-Krook[20] collision operator, and integrating over the perpendicular velocity give

$$f_1(v_{||}) = \sum_{n=-\infty}^{\infty} e^{-k_\perp^2 v_T^2/\Omega^2} I_n\left(\frac{k_\perp^2 v_T^2}{\Omega^2}\right)\frac{n_1}{n_0}kT_e \times \frac{ik_{||}\dfrac{\partial f_0}{\partial p_{||}} + \left(\dfrac{in\Omega}{kT_\perp} + \dfrac{\nu}{kT_e}\right)f_0}{\nu + ik_{||}v_{||} - i\omega - in\Omega}, \quad (2)$$

where Ω is the ion cyclotron frequency, I_n is the modified Bessel function of the first kind, and ν is the collision frequency. At a given frequency, then, there is a range of modes present in the plasma, each with its own $k_\perp$ and $k_{||}$ corresponding to an f_1 given by Eq. (2). Similarly, in Fig. 3, SVD resolves a subset of different modes for each given frequency and so we have separated the different spatial plasma modes with a localized measurement.

We give two examples of spatial mode separation, the first without Eq. (2) and the second with Eq. (2). The chamber ion acoustic longitudinal bounded mode is the ≈1250 Hz peak and is strong across all modes. A similar ion acoustic longitudinal mode bounded by the wire mesh grid is at ≈1650 Hz and is separated by SVD into the second and fourth most important principal axes.

The principal axes of the SVD provide a way to categorize these modes via comparison with Eq. (2). Since the matrix $\tilde{S}$ is Hermitian, SVD reduces to an eigenvector decomposition and thus the principal axes are the complex valued eigenvectors of the ion velocity fluctuation distribution function. A set of these eigenvectors is displayed in Fig. 4 for $f = 800$ Hz. By fitting these against Eq. (2) evaluated with the measured plasma parameters, we can categorize these modes. The resulting vectors from this fit are overlaid with dotted Argand diagrams for the two strongest modes in Fig. 4. The second strongest mode at top right in Fig. 4 corresponds to the spatially largest mode of the plasma

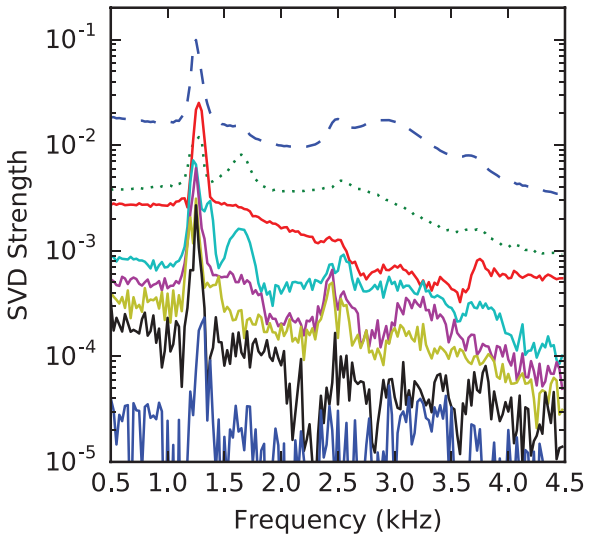

FIG. 3. Power spectra from connecting the singular values of the Hermitian matrix. A separate SVD is run on each 2D velocity space and connecting the singular values across frequency gives this plot. The fact that these power spectra differ is evidence of distinct modes. The third strongest mode, in solid red, becomes the second strongest around 1250 Hz and then drops back to being the third strongest. These are the velocity space degrees of freedom of plasma fluctuations as a function of frequency.

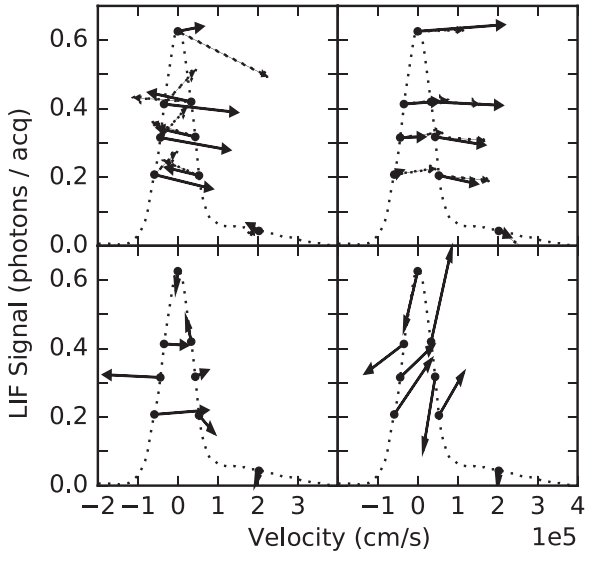

FIG. 4. Eigenvectors of the four strongest singular value modes (strongest at top left and going clockwise) at $f = 800$ Hz. Each vector component is complex valued and represented with a solid Argand diagram with origin at the measurement point on the deconvolved ion velocity distribution function. The Argand diagrams from Eq. (2) are shown with dashed lines for the two strongest modes for comparison. The strongest mode's Argand diagram describes a traditional linearized ion acoustic resonance.

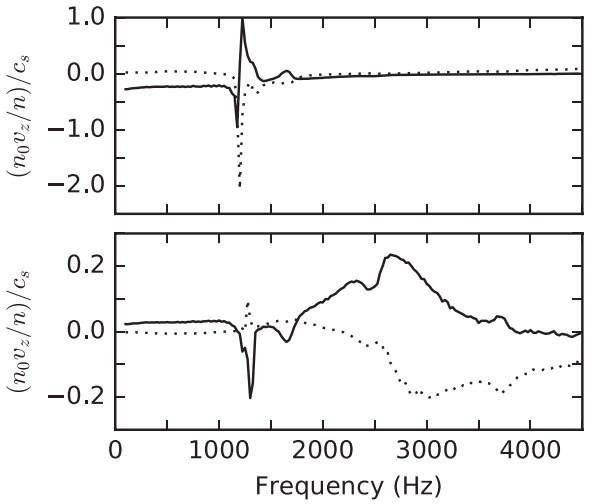

FIG. 5. Normalized admittance of the eigenmodes as a function of frequency. Top is the strongest eigenmode, while bottom is the second strongest eigenmode. The real component is the solid line, while the imaginary is the dotted line.

chamber with $\lambda_{||} = 460\,\text{cm}$ and fits best. However, the strongest mode itself corresponds to a smaller spatial mode with $\lambda_{||} \approx 14.6\,\text{cm}$ and $\lambda_{\perp} \approx 1.4\,\text{cm}$ and does not fit as well. This is another example of spatial mode separation from a local measurement and that theory work is an avenue of future work to interpret this measurement properly.

These mode structures do not remain constant as a function of frequency and may also change in relative strength. By minimizing the difference in eigenvectors as frequency is varied, we can find the continuous path of evolution of eigenvectors. Thus, we determine if and when the relative strength of the mode changes as a function of frequency. This process shows, for example, that the second and third modes in Fig. 3 switch in strength near 1250 Hz.

We introduce a generalized wave admittance by normalizing the appropriate eigenmode. In the case of the ion acoustic wave, combining the linearized force balance equation with the ion acoustic wave dispersion relation gives

$$\frac{n_0 v_z}{n} = c_s \sqrt{k_\perp^2 \frac{c_s^2}{\Omega^2 - \tilde{\omega}^2} + \frac{\omega}{\tilde{\omega}}}, \tag{3}$$

where $\tilde{\omega} = \omega - i\nu$. The left hand side can be calculated for each eigenmode by integrating the eigenvector to find the denominator n and the eigenvector's first velocity moment to find the numerator $n_0 v_z$. Figure 5 shows these admittances calculated using the two strongest data eigenmodes normalized to the ion acoustic speed c_s.

The admittances of Fig. 5 show that the second mode, which corresponds to modes constrained by the wire mesh grid, grows to reflect the larger $k_\perp$. The peak in the first mode corresponds to the plasma chamber bounded mode.

To summarize, we have introduced a new method for measuring the degrees of freedom and corresponding eigenmodes of plasma ion velocity distribution function fluctuations. This method uses a singular value decomposition in order to acquire the rank and the eigenmodes, in the case of a square Hermitian matrix, or the principal axes more generally. We show that this particular localized measurement gives the discrete set of modes, both bounded modes and kinetic modes, that constitute the plasma fluctuations. Analysis shows how these modes change in strength as a function of frequency. We also calculate a generalized wave admittance for each one of these eigenmodes.

The velocity space correlation function of the plasma distribution function given by this method makes it possible to measure phase space fluctuation spectra in terms of canonical velocity coordinates. Refinement of this method will be necessary since an integral transform to this end requires a nontrivial kernel.[21] A suggestive example is recent theoretical work finding phase space density fluctuation spectra and electric field spectra.[22] Alternatively, it should be possible to project the data matrix onto the basis of kinetic eigenmodes, which form a complete discrete spectrum for fluctuations in a weakly collisional plasma.[3]

This work was supported by the U.S. DOE under the NSF-DOE Program with Grant No. DE-FG02-99ER54543.

[1]N. G. Van Kampen, Physica **21**, 949 (1955).
[2]K. M. Case, Annals of Physics **7**(3), 349 (1959).
[3]C. S. Ng, A. Bhattacharjee, and F. Skiff, Phys. Rev. Lett. **92**, 065002 (2004).
[4]F. Skiff, H. Gunell, A. Bhattacharjee, C. S. Ng, and W. A. Noonan, Phys. Plasmas **9**, 1931 (2002).
[5]S. De Souza-Machado, M. Sarfaty, and F. Skiff, Phys. Plasmas **6**, 2323 (1999).
[6]A. Diallo and F. Skiff, Phys. Plasmas **12**, 110701 (2005).
[7]D. R. Hatch, P. W. Terry, F. Jenko, F. Merz, and W. M. Nevins, Phys. Rev. Lett. **106**, 115003 (2011).
[8]P. W. Terry, D. A. Baver, and S. Gupta, Phys. Plasmas **13**, 022307 (2006).
[9]P. W. Terry, K. D. Makwana, M. J. Pueschel, D. R. Hatch, F. Jenko, and F. Merz, Phys. Plasmas **21**, 122303 (2014).
[10]R. A. Stern and J. A. Johnson, Phys. Rev. Lett. **34**, 1548 (1975).
[11]A. Fasoli, F. Skiff, and M. Q. Tran, Phys. Plasmas **1**, 1452 (1994).
[12]I. Ü. Uzun-Kaymak and F. Skiff, Phys. Plasmas **13**, 112108 (2006).
[13]F. Anderegg, X.-P. Huang, E. Sarid, and C. F. Driscoll, Rev. Sci. Instrum. **68**, 2367 (1997).
[14]T. S. Strickler, T. K. Langin, P. McQuillen, J. Daligault, and T. C. Killian, Phys. Rev. X **6**, 021021 (2016); e-print arXiv:1512.02288.
[15]M. Sarfaty, S. De Souza-Machado, and F. Skiff, Phys. Rev. Lett. **80**, 3252 (1998).
[16]F. Skiff, C. S. Ng, A. Bhattacharjee, W. A. Noonan, and A. Case, Plasma Phys. Controlled Fusion **42**, B27 (2000).
[17]W. Horton, Rev. Mod. Phys. **71**, 735 (1999).
[18]C. Nardone, Plasma Phys. Controlled Fusion **34**, 1447 (1992).
[19]S. A. T. William, H. P. William, T. Vetterling, and B. P. Flannery, *Numerical Recipes*, 3rd ed. (Cambridge University Press, New York, NY, USA, 2007).
[20]P. L. Bhatnagar, E. P. Gross, and M. Krook, Phys. Rev. **94**, 511 (1954).
[21]P. J. Morrison, Phys. Plasmas **1**, 1447 (1994).
[22]P. J. Morrison and B. A. Shadwick, Commun. Nonlinear Sci. Numer. Simul. **13**, 130 (2008).